The rational design, synthesis and demonstration of the recognition and binding of a diaza-dioxa-12-crown-4 diphosphonate macrocycle to all crystal growth faces of barium sulfate

2 PERKIN

Dirk Bosbach,[a] Peter V. Coveney,[b] Jonathan L. W. Griffin,[c] Andrew Putnis,[a] Peter Risthaus,[a] Stephen Stackhouse[b] and Andrew Whiting*[c]

[a] *Department of Chemistry, University of Durham, Science Laboratories, South Road, Durham, UK DH1 3LE*
[b] *Centre for Computational Science, Queen Mary University of London, UK, E1 4NS*
[c] *Institut für Mineralogie, Universität Münster, Corrensstr. 24, 48149 Münster, Germany*

Received (in Cambridge, UK) 4th April 2002, Accepted 23rd May 2002
First published as an Advance Article on the web 13th June 2002

Computer-aided molecular design and virtual screening of a series of amino phosphonic acid derivatives were used to probe the probable interaction of these compounds as potential crystal growth inhibitors of barium sulfate, as judged by their ability to bind efficiently to all of the possible growing faces. As a result, a diphosphonic acid derivative of a 1,7-dioxa-4,10-diaza-12-crown-4 system **5** was proposed as a potential inhibitor of barium sulfate crystallisation. A subsequent synthesis of this macrocycle was developed, together with other larger-ring oxa-aza crown derivatives. Macrocycle **5** proved to be a highly efficient inhibitor of barium sulfate crystal growth at a level of 0.096 mM, as evidenced by the changes brought about in crystal morphology. Work was therefore undertaken to probe the mechanism of action of **5** using adsorption isotherms, mixed flow reactor and atomic force microscopy (AFM) measurements. It was possible to show that **5** inhibits effectively in solution by covering the growing surfaces, as observed on the 001 surface, effectively inhibiting two-dimensional nucleation as well as monolayer-step growth.

Introduction

The control and inhibition of crystal growth play a major role in several contemporary technologies. The work reported here has been aimed at the problem of barium sulfate scale formation in off-shore oil production. Oil bearing rocks frequently contain barium ions which, when in contact with sulfate-containing liquids such as drilling fluids and sea water, precipitate insoluble barium sulfate crystals. These scales block well bores, pipelines and pores in the oil-bearing strata, thus reducing the oilfield productivity.[1]

The most commonly used inhibitors of the growth of these crystals are polyphosphonates of which the most widely studied are diphosphonates.[2] It is thought that through replacing sulfate groups by phosphonate groups in the growing barium sulfate crystal, the inhibitor prevents further deposition of inorganic material and therefore growth on that particular face. Molecular modelling can be used to simulate the docking of the organophosphonates onto various growth surfaces of barium sulfate, in much the same way as we have recently reported with ettringite.[3] This type of work has been carried out by Davey *et al.*[2,4] showing that modelling can be used to explain the order of efficiency of various phosphonate crystal growth retarders of barium sulfate. Despite the reliability of these molecular modelling techniques, the rational design of barium sulfate inhibitors has not been pursued. We therefore decided that a barium sulfate crystal growth inhibitor could be rationally designed with a view to subsequent preparation and testing of potentially potent new retarders; a strategy which proved remarkably successful and which was reported in preliminary form recently.[5] In this paper, we report the full details of the design, synthesis and demonstration of the mode of action of a new barium sulfate crystal growth inhibitor which acts upon all growing faces.

Results and discussion

Crystal morphology of barium sulfate and potential inhibitor modelling

The first step in the molecular design and molecular modelling process was to calculate the morphology of barium sulfate. This was achieved using the Bravais Friedel Donnay Harker (BFDH) algorithm;[6] a method which is best regarded as empirical since it neglects the energetics of ion attachment. However, relative growth rates of the surfaces displayed in this first-order prediction were adjusted so as to match the observed morphology of the crystal. It could be seen which were the fastest growing surfaces, and therefore the ones which were most important to inhibit.

From these studies (Fig. 1) it was clear that barium sulfate adopts a simple rhombic morphology with large (001) faces connected by (210) sides; the latter being the fastest growing of the two. However, Hartman and Perdock[7] have shown that six

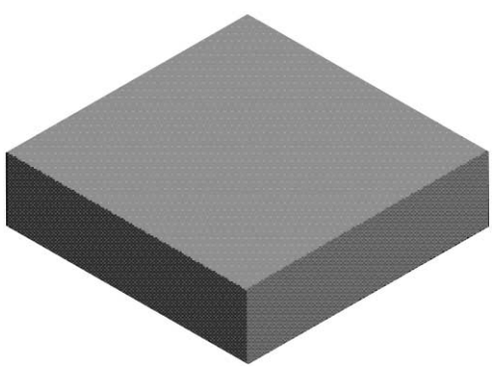

Fig. 1 A model of the rhombic morphology of barium sulfate.

 DOI: 10.1039/b203285f

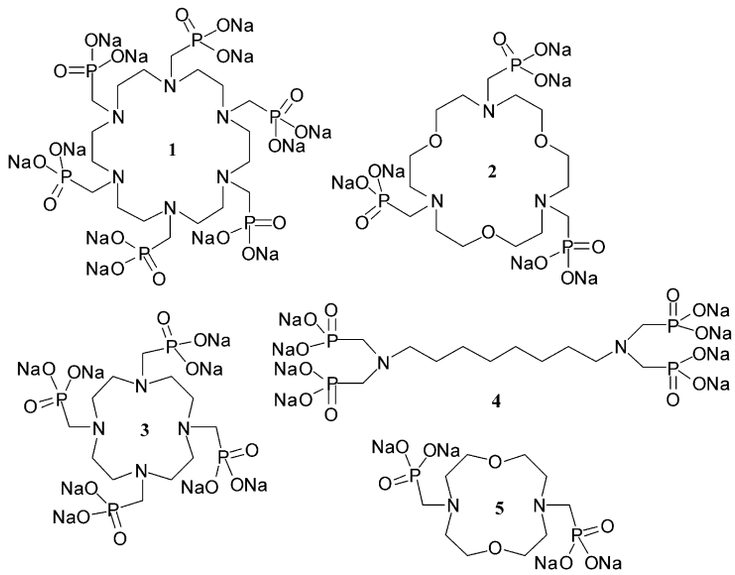

other faces are involved in the formation of these crystals. These are the (010), (101), (011), (111), (200) and (211) faces. Previously, inhibitors have only been modelled on one or two crystal faces of barium sulfates; however, if a retarder is capable of disrupting the growth of *all* eight important faces then, it should have even more powerful properties.

It has been shown by Coveney[8] in some recent molecular modelling studies that macrocyclic phosphonates are promising potential inhibitors of the nucleation and growth of the mineral ettringite. The ettringite system is similar to that of barium sulfate in that it is proposed that phosphonate retarders are used to replace sulfate ions on the growing crystal surface, preventing further crystal growth.[3] It was therefore decided that a series of different acyclic and macrocyclic phosphonates should be compared by testing for their approximate, relative potential activity as crystal growth inhibitors of barium sulfate using the CERIUS[2] molecular modelling package.[9]

Firstly the macrocycles reported to work as crystal growth retarders of ettringite, hexaphosphonic acid **1** and triphosphonic acid **2** were tested. This was achieved computationally by cleaving all of the eight faces of barium sulfate, the (001), (010), (101), (011), (111), (200), (210) and (211), from the crystal, and then superimposing each of the macrocycles (after geometry minimisation using the Dreiding force-field[10]) on these faces. This gave a crude yet effective first approximation as to whether the phosphonic acid groups in the additives would be capable of replacing the sulfate groups in the crystal lattice. Unfortunately, neither of the macrocycles **1** or **2** seemed to possess the geometry allowing superimposition of more than two phosphonate groups directly onto lattice sulfate groups, at any one time, on any of the faces. This suggested that these compounds were not going to be active crystal growth retarders in the barium sulfate system, as they are in that of ettringite.[3] Several other phosphonates were also assessed for their potential potency as barium sulfate inhibitors, two of which were **3** and **4**.

Tetraphosphonate **4** was found to be a particularly effective retarder of barium sulfate growth in the studies performed by Davey *et al.*,[2b] however, it was interesting to note that whilst this compound possessed the correct geometry for superimposition on the major (210) and (001) faces, it lacked that required for the others. During the molecular modelling work associated with ettringite,[3] it was noted that hexaphosphonic acid **1** seemed conformationally rigid, whereas its triphosphonic acid counterpart **2** formed by the simple replacement of every other nitrogen heteroatom with oxygen proved to be very flexible, and therefore would allow conformational change during docking of the phosphonate groups into the crystal lattice. Hence, as

Table 1 Inter-sulfate distances in crystalline barium sulfate

Face	Distance between sulfate sites/Å
(001)	10.916
(010)	11.406
(011)	12.644
(101)	11.527
(111)	11.406
(200)	10.916
(210)	10.648
(211)	11.559

tetraphosphonic acid **3**, whilst possessing quite a good geometric fit on the surface of the crystal lattice, was also found to be rigid, its dioxa-diaza analogue **5** was constructed. After geometry minimisation using the Dreiding force-field, diphosphonic acid **5** seemed to have an inter-phosphonate distance similar to at least one sulfate–sulfate distance on all eight of the above-mentioned faces. The inter-phosphonate distance is 10.925 Å and can be compared to the inter-sulfate group distances in Table 1.

In order to obtain a more accurate conformation of this macrocyclic diphosphonate, the semi-empirical molecular orbital package MOPAC,[11] implementing the PM3 Hamiltonian approximation method, was used yielding an inter-phosphonate distance on the inhibitor of 11.527 Å. Although this figure is slightly larger than that before the molecular orbital calculation, both phosphonate groups still seemed to coincide well with sulfate groups on all eight of the faces in Table 1. We might therefore have expected this macrocycle **5** to be an effective barium sulfate crystal growth inhibitor.

Although the simple geometric modelling described herein shows that the phosphate–phosphate distance on the potential inhibitor **5** matches up well with the sulfate–sulfate distances on the barium sulfate crystal, the actual conformation of the phosphonate was not optimised for docking into vacant sulfate sites. To allow for the possibility of conformational change of the phosphonate during docking, *i.e.* interaction between the retarder and the surface of barium sulfate, Rappe's universal force field[12] was used. Clearly it would have been desirable to have had a force field developed specifically for simulating the diphosphonate–crystal surface interaction, but since this type of interaction is dominated by electrostatic and steric factors, the present parameterisation was thought to be adequate for the purpose of this study.

Minimisation using the universal force field was performed, for each face, on a slice of barium sulfate not less than 12 Å deep, and 25 Å wide. This was to ensure that the edges of the

crystal lattice were further than 8.5 Å (spline cut-off distance) from any point on the inhibitor, thus ruling out the possibility of any edge effect. There also had to be vacant sites in the surface onto which the adsorbing molecule could dock. This was achieved by the removal of the two sulfate groups which the inhibitor proposed to replace, and these positive sites could then be filled by the negatively charged phosphate groups during minimisation. The inhibitor **5** was then positioned on the crystal surface so that the phosphonate groups were as close to the "positive holes" as possible and minimisation could then take place.

Once this had been achieved, molecular dynamics was performed on the new surface. The simulations were run at a constant temperature of 300 K for 10,000 steps using an integration step size of one femtosecond. Whereas some others[4] allowed the top layer of the crystal to relax during minimisation, the whole crystal lattice, in this case, was fixed. There are two reasons for doing this. Firstly, the non-periodicity of the combined molecule-plus-crystal unit meant that different parts of the selected portion of the crystal structure do not experience the same local coulombic potential, which would lead to collapse of the structure if the lattice atoms were not fixed, secondly because crystal growth is a slow process compared with the time-scales of interest for the molecular dynamics of phosphonate retarders. Note that the biggest implicit assumption here is that the barium sulfate crystal growth nuclei are well represented by the crystal structure of barium sulfate.[8] The purpose of the molecular dynamics simulation was to ensure that optimal molecular conformations were located that might otherwise have been missed by trapping in local minima during the energy minimisation procedure. However, this yielded little or no change in the conformation of the potential retarder **5**, and it was therefore presumed that an optimum conformation had been reached. The results of the minimisation and molecular dynamics of the inhibitor on all of the eight important growth faces in barium sulfate are shown in Figs. 2–7.

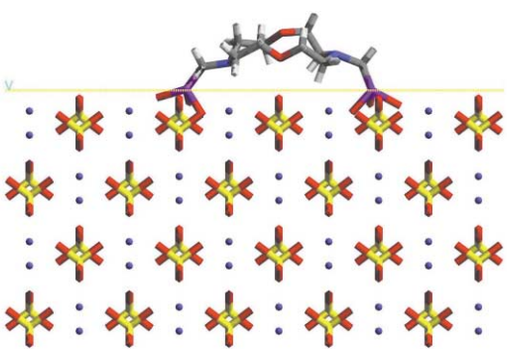

Fig. 2 Potential inhibitor **5** docked onto the (001) face of barium sulfate.

The results of the energy minimisations confirmed the expectations of the simple geometric analysis. In all cases, major conformational changes in the potential retarder **5** occurred during the docking procedure. In all of the minimisations, arching of the macrocycle occurred as the phosphate groups shifted into place in the crystal lattice. This seemed to happen by virtue of the presence of the macrocyclic oxygens[8] which gives added flexibility to the macrocyclic ring during docking. Also, because of the supple nature of the macrocycle, in the cases where the sulfate–sulfate distances (in particular the (001), (200) and (210) faces) are smaller than the intramolecular phosphate–phosphate distance of the retarder, arching during minimisation occurs more readily, thus adjusting the phosphate–phosphate distance to suit the surface requirements of that particular face.

As previously demonstrated,[8] therefore, when designing additives their flexibility is crucial at the molecular modelling level,

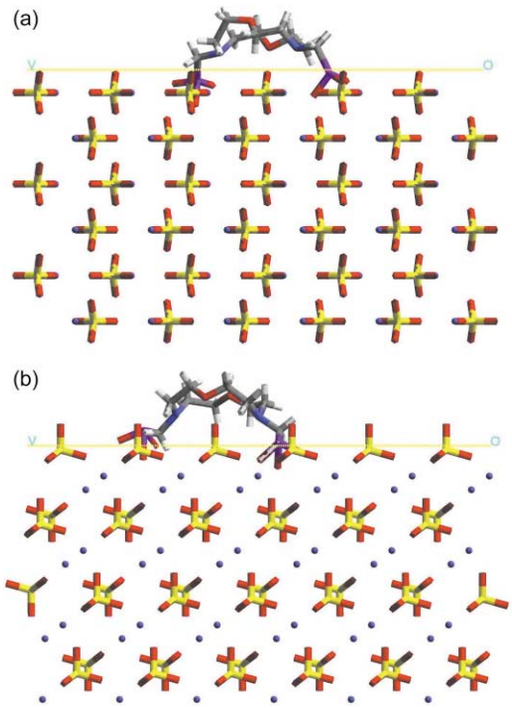

Fig. 3 (a) Potential inhibitor **5** docked onto the (010) face of barium sulfate. (b) Potential inhibitor **5** docked onto the (011) face of barium sulfate.

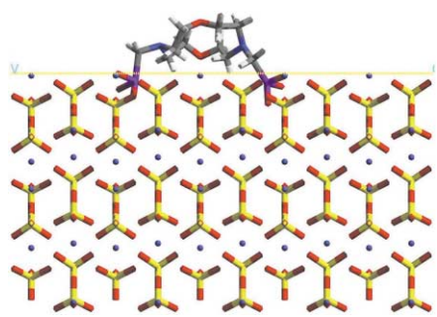

Fig. 4 Potential inhibitor **5** docked onto the (101) face of barium sulfate.

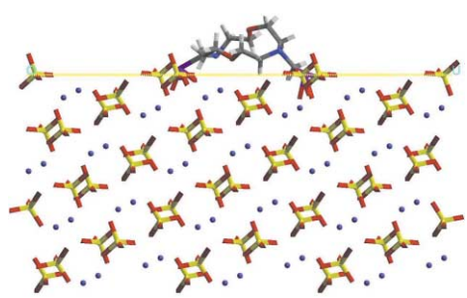

Fig. 5 Potential inhibitor **5** docked onto the (111) face of barium sulfate.

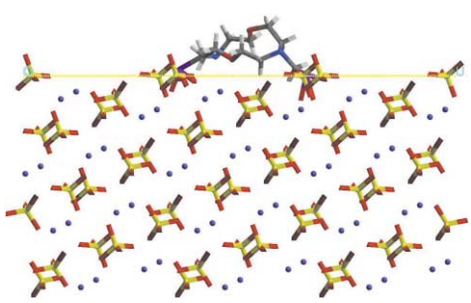

Fig. 6 Potential inhibitor **5** docked onto the (200) face of barium sulfate.

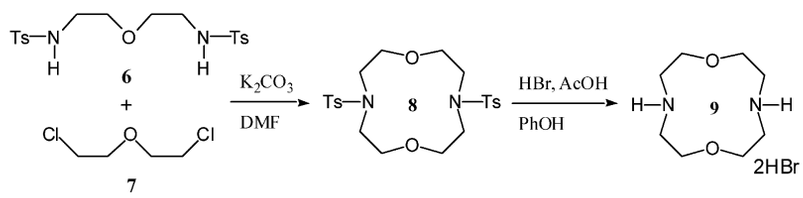

Scheme 1

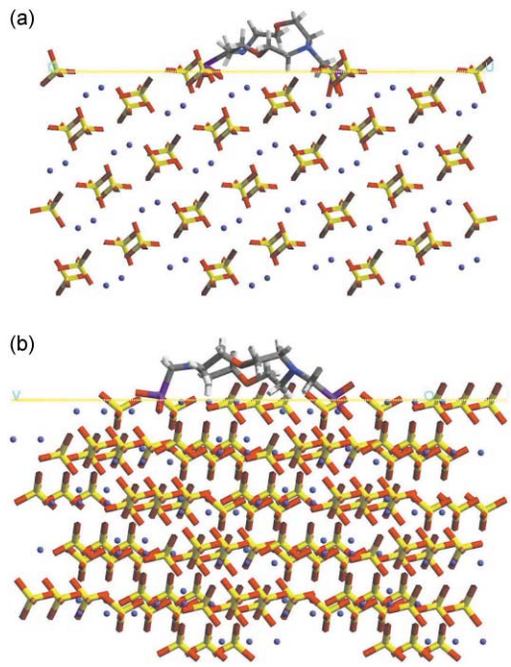

Fig. 7 (a) Potential inhibitor **5** docked onto the (210) face of barium sulfate. (b) Potential inhibitor **5** docked onto the (211) face of barium sulfate.

and it seems that, potentially, this inhibitor **5** could be very powerful. However, there was no guarantee that in the actual barium sulfate system, this retarder **5** would be effective at all, let alone more effective than inhibitors which have not been rationally designed. It was therefore to the empirical validation of this molecule's efficacy that we turned next.

Macrocycle synthesis

There are several possible synthetic routes leading to the parent macrocycle **9**[13] of the inhibitor in question, **5**. The most attractive is a modified version of the route taken by Bogatsky *et al.*,[14] mainly due to the availability of starting materials and well documented chemistry.

Cyclisation of dichloride **7** and ditosylamine **6** (dichloride **7** was used to access starting material **6** using literature methods[15]) in a mixture of toluene and water, using lithium hydroxide and tetra-*n*-butylammonium iodide (phase transfer catalyst) proved to be troublesome on work-up. However, when potassium carbonate was used in DMF (0.05 M, 100 °C, 7 hours) (Scheme 1), the reaction mixture could be simply filtered, evaporated and recrystallised to give the required compound **8** in 60% yield. Deprotection of the amine was attempted initially *via* reduction with lithium aluminium hydride which proved unsuccessful; however, detosylation was achieved by utilising Atkins' method[13a] to give the di-HBr salt of macrocycle **9**, which could be precipitated with either acetone or ethanol after removal of the solvent.

Despite the successful preparation of macrocycle **8** as shown in Scheme 1, it is noteworthy that when dichloride **7** and ditosylamine **6** are reacted at higher concentrations in DMF (0.2 M) substantially less of the 12-crown-4 derivative **8** (43%) was obtained and examination of the mother liquors by NMR showed that two further macrocycles had been produced. The main component (46% by ^{1}H NMR) was found to be the 24-membered ring **10**,[16] while the minor component was the previously unknown 36-membered ring **11**.

The exact identity of each of the larger macrocycles **10** and **11** was not initially obvious, since they contain the same basic repeat units. However, fast-atom bombardment (FAB) and electrospray mass spectrometric analysis of the mother liquors allowed detection of the larger rings. When FAB was used, the $(M + H)^+$ ion was detected for both the 24-crown-8 **10** (*m*/*z* 965) and the 36-crown-12 **11** (*m*/*z* 1447) macrocycles. Similarly, in the presence of a solution of KI, FAB indicated the presence of both of the larger rings; a peak at *m*/*z* 1003 produced by $(M + K)^+$ of **10**, and a peak at *m*/*z* 1485 from the $(M + K)^+$ ion of **11**. When electrospray was used, the formation of the 24-crown-8 ring during the reaction was confirmed by the presence of peaks at *m*/*z* 965, 987 and 1003 corresponding to $(M + H)^+$, $(M + Na)^+$ and $(M + K)^+$ respectively. A weak signal at *m*/*z* 1469, corresponding to $(M + Na)^+$, indicated again that the 36-crown-12 ring was also formed during the reaction.

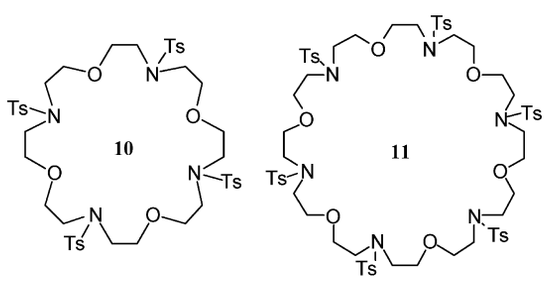

After the initial removal of the 12-crown-4 derivative **8** from the reaction mixture, it was found that the isolation of **10** was possible by recrystallisation from acetic acid. Deprotection of this tetratosylated macrocycle **10** could be achieved in 76% yield as shown in eqn. (1). Further analysis of the product **12** allowed the unambiguous structural assignment of starting tetratosylate **10**.

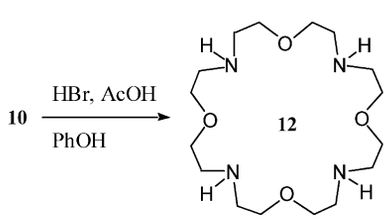

(1)

Attempts to isolate the 36-membered ring **11** were less successful. After multiple recrystallisations using different solvent systems and various column techniques, including silica gel, reverse phase and preparative HPLC, it was found that the separation of the macrocycle **11** from residual macrocycle **10** was not possible.

Arising from this production of macrocycles **8**, **10** and **11**, several points are particularly noteworthy: 1) the combined overall yield of the macrocycles **8**, **10** and **11** was greater than 95%, showing the remarkable efficiency of the reaction; 2) there are several syntheses of related 24-membered crown systems

using a macrocyclisation strategy which involves formation of up to four new bonds,[16,17] however this example is particularly efficient and heavily dependent upon the reaction concentration (*vide infra*); 3) 36-membered ring macrocycles are generally formed from a single acyclic precursor and there are no comparable examples of the formation of such rings in a one-pot process requiring the formation of four or more new bonds;[17c] 4) the efficiency of the formation of the 24- and 36-membered rings is remarkable, and concentration and only partially metal cation dependent, as illustrated by carrying out the identical reaction with caesium carbonate in place of potassium carbonate, which did not radically change the product distribution or yields. Both lithium and sodium carbonate failed to promote any discernible reaction at all. Furthermore, if the reaction was carried out at higher dilution (5 mM), after 4 days the reaction only proceeded to 50% conversion and only the 12-membered ring **8** was produced. The dependence of the formation of **10** on both the presence of a suitable template and the concentration suggests that these phenomena strongly affect the conformation of the acyclic oligomers. At higher reactant concentrations, the various effects seem to work in concert to enable efficient chain extension, rather than smaller ring formation. It is possible that relatively highly organised, possibly helical structures are responsible for these types of effects.

Returning to our main theme, once macrocycle **9** had been obtained, attempted alkylation could then proceed with a view to synthesising diphosphonic acid **5**. Synthesis of the diethyl ester **13** was initially attempted.

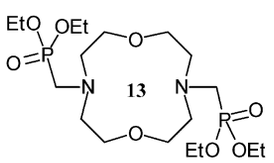

Diethyl phosphite, paraformaldehyde and azacrown **9** were reacted in benzene with azeotropic removal of water; despite the formation of **13**, the yield was low. Hence direct reaction to the phosphonic acid was employed using the same reagents and conditions reported previously [eqn. (2)].[3] The diphosphonic acid analogue of **5** was obtained by crystallisation of the di-HCl salt from the reaction mixture using acetone in almost quantitative yield. This was then converted into the sodium salt by buffering with sodium hydroxide followed by precipitation.

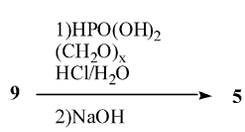

(2)

Mechanism of inhibition of barium sulfate crystal growth

In order to test the inhibitory activity of macrocycle **5** the method of Davey *et al.*[2b] was used, together with scanning electron microscopy (SEM) to observe the effect of varying concentrations of the inhibitor upon barium sulfate morphology, compared with other commercial inhibitors. At a loading of 0.096 mM of added inhibitor **5**, we found spherical single crystals with no evidence of facetting using SEM.[5] In order to probe the mode of action of compound **5** more fully, we turned to examining adsorption isotherms, mixed flow reactor and atomic force microscopy (AFM) measurements.

Adsorption isotherms. The adsorption behaviour of **5** onto barite as a function of inhibitor concentration and pH was studied in batch experiments at room temperature (21 °C). We used synthetic barite powder from Sigma Aldrich, which was treated with concentrated nitric acid for 24 h. The N_2-BET surface area of the treated powder is 2.8 m^2 g^{-1}.[18] The inhibitor adsorption was determined from barite suspensions with 0.5 g barite/100 ml. The phosphonate concentration in solution was analysed after extracting the aqueous phase from the suspension after 48 h with a syringe filter (pore size: 0.45 μm).

The barite surface coverage with **5** clearly increases with increasing inhibitor concentration in solution (Fig. 8). Comparative studies with HEDP (1-hydroxyethylene-1,1-diphosphonic acid), a well known inhibitor[19] for various scale minerals including calcite, gypsum and barite, showed a higher surface coverage after 48 h for a given inhibitor concentration. Although HEDP and **5** both have two phosphonate functional groups, the conformational flexibility of HEDP is very limited compared to **5**. Surface coverage is higher at higher pH for both HEDP and **5**, which is probably due to a higher deprotonation state at high pH. The adsorption behaviour was found to be independent of the ionic strength of the solution.

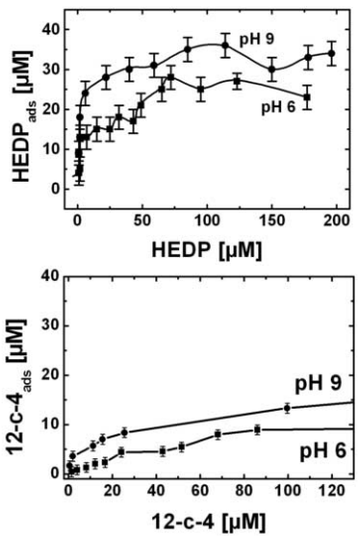

Fig. 8 Barite inhibitor adsorption behaviour as a function of concentration and pH for HEDP (top) and the 12-crown-4 diphosphonate **5** (bottom) at room temperature.

Mixed flow reactor experiments. In order to compare the performance of inhibitor **5** under well defined conditions, we have performed mixed-flow reactor (MFR) experiments at a defined supersaturation IAP/K = 40, where IAP is the ion activity product $a_{Ba^{2+}}$ $a_{SO_4^{2-}}$ and K the solubility product of barite ($10^{-9.96}$ mol^2 L^{-2}). BET surface-area-normalized crystal growth rates were obtained under steady-state conditions (Fig. 9). For the MFR experiments we used fine grained natural barite powder (hydrothermally formed) after various preparation steps including sieving, magnetic separation and gravity concentration. After these separation steps SEM observations as

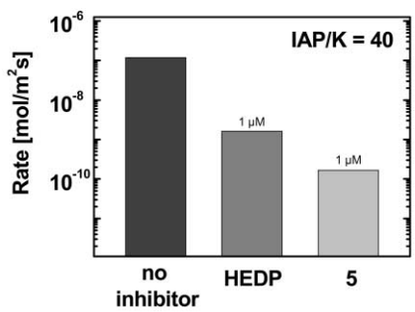

Fig. 9 BET surface-area-normalised crystal growth rates obtained from mixed-flow reactor experiments performed on native barite and barite in the presence of micromolar solutions of HEDP and our 12-crown-4 diphosphonate **5**, showing the efficacy of the latter compound under these conditions.

well as ICP analysis showed no significant contamination by intergrown minerals (such as quartz) and trace elements. The grain size varied between 63–200 μm. The specific surface area of the barite powder used for the MFR experiments was 0.5 m^2 g^{-1} (determined *via* N_2-BET). The reactor had a volume of 150 ml and was operated with a pump rate of 20 ml min^{-1}.

The growth rate in pure $BaSO_4$ solution at a supersaturation of 40 without inhibitor is about 1.5×10^{-7} mol m^{-2} s^{-1}. A significant retardation of the growth rate, by 2–3 orders of magnitude, can be observed in the presence of only 1 μM of HEDP (1.5×10^{-9} mol m^{-2} s^{-1}) and inhibitor **5** (1.5×10^{-10} mol m^{-2} s^{-1}) at the same degree of supersaturation. Inhibitor **5** is even more efficient as a barite crystal growth inhibitor than HEDP under these conditions. This is surprising since HEDP shows a higher surface coverage (see Fig. 8). However, from a kinetic perspective, the adsorption of inhibitor **5** could be faster than that of HEDP.

Atomic force microscopy observations. Barite growth was observed *in situ* on a molecular level using a Digital Instruments Nanoscope III Multimode AFM operating in contact mode at room temperature with a commercially available fluid cell. Si_3N_4 cantilevers of length 100 μm with integrated pyramidal TwinTip™ tips were used (spring constant: 0.6 N m^{-1}). Freshly cleaved, optically clear natural barite crystals from various locations were mounted in a cup-like Teflon sample holder with an adhesive. Before running the actual growth experiments, the sample was initially exposed to deionised water in order to dissolve and clean the topmost mineral surface layer, thus reducing the risk of surface contamination which could affect the growth experiment.

Fig. 10 shows an AFM image of a barite (001) surface imaged

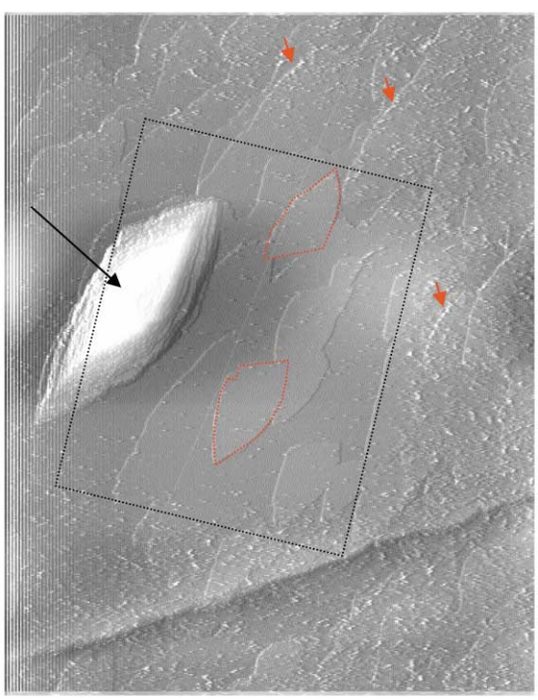

Fig. 10 Atomic force microscopy image of a barite (001) surface in a supersaturated solution (IAP/K = 20, 0.1 mol L^{-1} NaCl) with 50 μM inhibitor **5** at room temperature (scan area: 7 × 7 $μm^2$). A growth spiral as well as islands associated with two-dimensional nucleation are visible. See text for further discussion.

in situ at a supersaturation of IAP/K = 20 (pH = 5.8, ionic strength: 0.1 mol L^{-1} adjusted with NaCl) and an inhibitor concentration up to 50 μM. One can clearly see monomolecular steps with a step height of 0.35 nm representing a single structural $BaSO_4$ layer, which is typical for a barite (001) surface exposed to a supersaturated solution.[20,21] Furthermore, a growth spiral (indicated by an arrow) can be seen, with a typical morphology for the conditions used in the experiment.[22] Islands associated with two-dimensional nucleation with a height of one $BaSO_4$ layer exhibit a typical sector morphology.[20,21]

The central area of the AFM image in Fig. 10 (indicated by a rectangle) represents an area which was scanned with a high loading force (> 100 nN). Under these conditions, the AFM tip was used as a tool which scratched off a surface coating, most likely the adsorbed inhibitor. After reducing the loading force below 10 nN and imaging a larger scan area, the "cleaned" inhibitor-free surface area could be observed.

Another interesting feature in the inhibitor-covered surface regions is the apparent enrichment of inhibitor along monolayer step edges (Fig. 10, indicated by red arrows). This indicates a preferential and selective attachment to these surface sites and that these sites are more reactive compared to flat terraces. However, the crystallographic orientation of the monolayer step edges as well as the morphology of 2D islands is identical to that obtained under inhibitor-free conditions. A change in island morphology would suggest that the inhibitor molecule "prefers" certain step edge sites over other sites: such selectivity can be excluded based on our AFM observations.

Summary and conclusions

Molecular modelling led to the design of novel 12-crown-4 diphosphonate **5** which purported to interact strongly with all growth surfaces of barium sulfate. Subsequent selective synthesis of **5** was achieved under template and concentration dependent conditions and initial SEM studies confirmed the effectiveness of this compound. More detailed adsorption, mixed flow reactor and AFM studies were then carried out. These data enable us to conclude that although **5** does not adsorb onto barium sulfate in the same way as the much studied inhibitor HEDP does (under equilibrium conditions), it nevertheless inhibits more effectively in solution at the same inhibitor concentration. It is possible that kinetic effects may explain the inhibition performance of **5**. Our AFM observations indicate that the barite (001) surface eventually becomes covered with **5**, effectively inhibiting two-dimensional nucleation as well as monolayer-step growth. Therefore, by combining macroscopic experimental data with microscopic AFM *in situ* observations, we have been able to confirm the predicted high efficiency of **5** for barite crystal growth. It is clearly important to understand the origin of the kinetic effects which are operating between **5** and the barium sulfate surface, particularly to enable the improved design of new surface-recognition agents.[23] Studies directed towards such an understanding will be the subject of future work, in addition to a more in depth understanding of the extraordinarily efficient macrocyclisation reactions leading to **8**, **10** and **11** and the effects of concentration, templates and conformation upon the selectivity.

Experimental

All reagents which were not prepared as detailed later were purchased from either Aldrich, Acrös Chimica, Avocado or Lancaster, with the exception of hexaphosphonic acid **1** which was kindly donated by Schlumberger Cambridge Research. All were used without any further purification unless otherwise stated. Solvents were all distilled before use over either benzophenone/sodium (THF) or calcium hydride (all remaining solvents) under an atmosphere of argon.

T.l.c. was performed on Merck plastic or aluminium sheets coated with silica gel 60 F_{254} (Art. 5735); the chromatograms were initially examined under u.v. light and then developed either with iodine vapour or a 10% ethanolic solution of molybdophosphoric acid and visualised by heating with a heat gun. Column chromatography was achieved under medium

pressure, using Acrös Chimica silica gel, 0.035–0.07 nm (pore diameter: *ca.* 6 nm).

All anhydrous, low temperature reactions were carried out in glassware which was dried prior to use by storage in a glass oven maintained at 140 °C and cooled under a stream of argon. Evaporations were carried out using a Büchi rotary evaporator or Büchi cold-finger rotary evaporator. Kugelröhr distillations were carried out using a Büchi GKR-51 Kugelröhr apparatus. Melting points were determined using an Electrothermal melting point apparatus and are uncorrected. ^{1}H NMR spectra were recorded at 200 or 300 MHz on a Bruker AC200 or AC300 spectrometer. ^{13}C NMR spectra were recorded at 75.5 MHz on a Bruker AC300 spectrometer. Both ^{1}H and ^{13}C spectra were recorded using either $CDCl_3$ ($CHCl_3$) or DMSO as internal standards respectively. Infrared spectra were recorded on a Perkin-Elmer 783 equipped with a PE600 data station or a Perkin-Elmer 1605 FT-IR and ultraviolet spectra were recorded on a Perkin-Elmer 115 spectrometer. Electron impact (EI) (70 eV) and chemical ionisation (CI) spectra were recorded with a Kratos MS25. Fast atom bombardment (FAB) spectra were recorded on a Kratos MS50, using a *m*-nitrobenzyl alcohol matrix and accurate mass determinations were carried out on a Kratos Concept IS spectrometer.

Preparation of cyclic ditosylamide 8

Ditosylamide **6** (10.24 g, 24.80 mmol) and potassium carbonate (27.40 g, 0.20 mol) were dissolved in DMF (500 ml) and treated with dichloride **7** (3.55 g, 24.80 mmol) (dropwise addition). The reaction mixture was then heated to 100 °C and left to stir for 16 hours and the solvent evaporated. To the remaining solid, DCM (100 ml) was added, the mixture filtered through Celite, the solid residue was washed with DCM (2 × 50 ml), the organic fractions combined and evaporated. The remaining white solid was then dissolved in hot toluene, from which the required compound **8** precipitated on cooling as a white solid (7.20 g, 60%); mp 202–204 °C.[15] All spectroscopic and analytical properties were identical to those reported in the literature.[15]

Preparation of cyclic tetratosylamide 10

A stirred mixture of ditosylamide **6** (0.10 g, 0.24 mmol), potassium carbonate (0.20 g, 1.46 mmol), DMF (1 ml) and dichloride **7** (35 mg, 0.24 mmol) was heated to 100 °C and for 16 hours. After evaporation of the solvent, the remaining solid was resuspended in DCM (100 ml) and filtered through Celite. The residue was washed with DCM (2 × 5 ml), the organic fractions combined and evaporated. The remaining white solid was then dissolved in hot toluene from which the 12-crown-4 oligomer **8** precipitated, which was removed by filtration (0.059 g, 50%) and the toluene was re-evaporated. The remaining white solid was then recrystallised from hot acetic acid giving tetratosylate **10** as a white solid (0.11 g, 48%); mp 144–146 °C; λ_{max} 230.6 (ε = 41339) nm; ν_{max} (KBr) *inter alia* 1345 (asym SO_2), 1165 (sym SO_2) cm^{-1}; δ (^{1}H, 300 MHz, $CDCl_3$) 2.42 (12H, s, 4 × C*H*$_3$), 3.30 (16H, t, *J* = 5.5 Hz, 8 × NC*H*$_2$), 3.53 (16H, t, *J* = 5.5 Hz, 8 × OC*H*$_2$), 7.30 (8H, d, *J* = 8.1 Hz, 8 × CH_3CC*H*), 7.67 (8H, d, *J* = 8.1 Hz, 8 × SO_2CC*H*); δ (^{13}C, 75.5 MHz, $CDCl_3$) 21.45 (4 × *C*H$_3$), 49.11 (8 × NCH$_2$), 70.27 (8 × OCH$_2$), 126.99 (8 × CH_3C*C*H), 129.71 (8 × SO_2C*C*H), 136.50 (4 × CH_3*C*), 143.39 (4 × SO_2*C*); *m*/*z* (+ve FAB) *inter alia* 809 (M − ArSO$_2$)$^+$, 965 (M + H)$^+$, 1003 (M + Na)$^+$; accurate mass, calc. for $C_{44}H_{60}N_4O_{12}S_4^+$ *m*/*z* 965.3246, found 965.3152.

Preparation of cyclic diamine 9

Cyclic ditosylamide **8** (2.13 g, 4.44 mmol) and phenol (2.50 g, 26.60 mmol) were dissolved in 33% HBr/AcOH (133 ml) and stirred. The reaction mixture was then heated to 80 °C and left for 60 h. After this time the reaction was cooled and the solvent was removed to a volume of 20 ml, when 100 ml acetone were then added to precipitate the HBr salt of **9** which was then filtered, washed with acetone (3 × 50 ml) and dried under vacuum yielding the di-HBr salt of diamine **9** (1.23 g, 3.66 mmol, 83%); ν_{max} (KBr) *inter alia* 3480 (NH) cm^{-1}; δ (^{1}H, 300 MHz, D_2O) 3.46 (8H, t, *J* = 5.1 Hz, 4 × NC*H*$_2$), 3.92 (8H, t, *J* = 5.1 Hz, 4 × OC*H*$_2$); δ (^{13}C, 75.5 MHz, D_2O) 48.14 (4 × NCH$_2$), 66.14 (4 × OCH$_2$); *m*/*z* (+ve FAB) *inter alia* 175 (M + H)$^+$; accurate mass, calc. for $C_8H_{19}N_2O_2^+$ *m*/*z* 175.1446, found 175.1442.

Preparation of cyclic tetraamine 12

Cyclic tetratosylamide **10** (0.20 g, 0.14 mmol) and phenol (0.23 g, 2.49 mmol) were dissolved in 33% HBr/AcOH (5 ml) and stirred. The reaction mixture was then heated to 80 °C and left for 60 h. After this time the reaction was cooled and the solvent was removed to a volume of 1 ml, when 5 ml acetone were added to precipitate the HBr salt of **12** which was then filtered, washed with DCM (3 × 10 ml) and dried under vacuum yielding the tetra-HBr salt of tetraamine **12** (0.11 g, 76%); mp 132–134 °C; ν_{max} (KBr) *inter alia* 3480 (NH) cm^{-1}; δ (^{1}H, 200 MHz, D_2O) 3.47 (16H, t, *J* = 4.9 Hz, 4 × NC*H*$_2$), 3.97 (16H, t, *J* = 4.9 Hz, 4 × OC*H*$_2$); δ (^{13}C, 75.5 MHz, D_2O) 48.65 (8 × NCH$_2$), 66.57 (8 × OCH$_2$); *m*/*z* (+ve FAB) *inter alia* 349 (M + H)$^+$; accurate mass, calc. for $C_{16}H_{37}N_4O_4^+$ *m*/*z* 349.2815, found 349.2826.

Preparation of cyclic diphosphonic ester 13

The di-HBr salt of cyclic diamine **9** (0.50 g, 1.49 mmol), diethyl phosphite (0.45 g, 3.27 mmol) and triethylamine (0.83 ml, 5.96 mmol) were dissolved in benzene (10 ml) which was then heated to reflux and left for 10 min. Then *para*-formaldehyde (0.13 g, 4.46 mmol) was added in small portions in benzene over 60 minutes whilst azeotropically removing water. The distillation apparatus was removed and replaced by a reflux condenser so that refluxing could continue overnight. The benzene was then removed and replaced by a mixture of water (10 ml) and dichloromethane (10 ml) the latter of which was removed and the water layer washed again with dichloromethane (2 × 10 ml). The organic fractions were pooled and the solvent removed to leave colourless oil **13** (0.31 g, 43%); ν_{max} (thin film) *inter alia* 1050 (P–O-alkyl), 1225 (P=O) cm^{-1}; δ (^{1}H, 200 MHz, $CDCl_3$) 1.28 (12H, t, *J* = 7.1 Hz, 4 × C*H*$_3$), 2.88 (8H, t, *J* = 5.7 Hz, 4 × NC*H*$_2$CH$_2$), 3.01 (4H, d, *J* = 9.5 Hz, 2 × PC*H*$_2$), 3.57 (8H, t, *J* = 5.7 Hz, 4 × OC*H*$_2$CH$_2$), 4.18 (8H, m, 4 × C*H*$_2$CH$_3$); δ (^{13}C, 75.5 MHz, $CDCl_3$) 16.32 (4 × *C*H$_3$), 47.12 (d, *J* = 149.0 Hz, 2 × PCH$_2$), 55.60 (4 × NCH$_2$CH$_2$), 61.79 (4 × OCH$_2$CH$_2$), 68.86 (4 × POCH$_2$); *m*/*z* (+ve FAB) *inter alia* 199 (M − 2 PO(OEt)$_2$)$^+$, 337 (M − PO(OEt)$_2$)$^+$, 475 (M + H)$^+$, 497 (M + Na)$^+$; accurate mass, calc. for $C_{11}H_{21}N_2O_8P_2^+$ *m*/*z* 475.2337, found 475.2343.

Preparation of cyclic diphosphonic acid di-HCl salt of 5

The di-HBr salt of diaza-12-crown-4 **9** (1.0 g, 2.98 mmol) and phosphonic acid (0.49 g, 5.95 mmol) were dissolved in a mixture of concentrated HCl (5 ml) and water (5 ml) and stirred. The mixture was then heated to reflux (~115 °C) and formaldehyde (0.97 ml of a 37% solution in water, 11.90 mmol) was added in small portions over 60 minutes. After addition, refluxing continued for 16 h at which point the reaction mixture was cooled and the solvent removed. On adding acetone (50 ml) with swirling, a white precipitate formed which was filtered. The white solid was then dried *in vacuo* to yield the di-HCl salt of **5** (1.28 g, 2.95 mmol, 99%); ν_{max} (KBr plate) *inter alia* 1133 (P=O) cm^{-1}; δ (^{1}H, D_2O) 3.58 (1H, d, *J* = 12.3 Hz, PCH$_2$), 3.66–3.92 (2H, m, NCH$_2$), 3.92–4.03 (2H, m, OCH$_2$); δ (^{13}C, D_2O) 53.1 and 54.9 (PCH$_2$), 57.0 (NCH$_2$), 65.4 (OCH$_2$); *m*/*z* (+ve FAB) 363 (M + H)$^+$, 385 (M + Na)$^+$, 407 (M + 2Na)$^+$, 429

$(M + 3Na)^+$; accurate mass, calc. for $C_{10}H_{24}N_2O_8P_2$ $(M + H)^+$ 363.1092, found 363.1086.

Acknowledgements

We are grateful to the Engineering and Physical Sciences Research Council (UK) and Schlumberger Cambridge Research for a Total Technology studentship award (to J.G.) (GR94007291).

References

1 W. J. Benton, I. R. Collins, I. M. Grimsey, G. M. Parkinson and S. A. Rodger, *Faraday Discuss.*, 1993, **95**, 281.
2 (*a*) S. N. Black, L. A. Bromley, D. Cottier, R. J. Davey, B. Dobbs and J. E. Rout, *Nature*, 1991, **353**, 540; (*b*) S. N. Black, L. A. Bromley, D. Cottier, R. J. Davey, B. Dobbs and J. E. Rout, *J. Chem. Soc., Faraday Trans.*, 1991, **87**, 3409.
3 (*a*) P. V. Coveney, R. J. Davey, J. L. W. Griffin and A. Whiting, *Chem. Commun.*, 1998, 1476; (*b*) P. V. Coveney, R. J. Davey, J. L. W. Griffin and A. Whiting, *J. Chem. Soc., Perkin Trans. 2*, 1999, 1979.
4 C. R. A. Catlow, R. J. Davey, D. H. Gay and A. L. Rohl, *J. Am. Chem. Soc.*, 1996, **118**, 642.
5 P. V. Coveney, R. Davey, J. L. W. Griffin, Y. He, J. D. Hamlin, S. Stackhouse and A. Whiting, *J. Am. Chem. Soc.*, 2000, **122**, 11557.
6 (*a*) A. Bravais, *Etudes Crystallographiques*, Gauthier-Villars, Paris, 1913; (*b*) G. Friedel, *Bull. Soc. Fr. Mineral.*, 1907, **30**, 326; (*c*) J. D. H. Donnay and D. Harker, *Am. Mineral.*, 1937, **22**, 463.
7 P. Hartman and W. G. Perdock, *Acta Crystallogr.*, 1955, **8**, 525.
8 P. V. Coveney and W. Humphries, *J. Chem. Soc., Faraday Trans.*, 1996, **92**, 831.
9 CERIUS and CERIUS^2, Molecular Simulations Inc., 1993.
10 W. A. Goddard III, S. L. Mayo and B. D. Olafson, *J. Phys. Chem.*, 1990, **94**, 8897.
11 J. J. P. Stewart, MOPAC Version 5.0, QCPE No. 455, Department of Chemistry, Indiana University, 1989.
12 A. Rappe, C. J. Casewit, K. S. Colwell, W. A. Goddard III and W. M. Skiff, *J. Am. Chem. Soc.*, 1992, **114**, 10024.
13 (*a*) J. Richman and T. J. Atkins, *J. Am. Chem. Soc.*, 1974, **96**, 2268; (*b*) J. Jurczak, S. Kaspryzk, P. Salanski and T. Stankiewicz, *Chem. Commun.*, 1991, 956; (*c*) L. Borjesson and C. J. Welch, *Acta Chem. Scand.*, 1991, **45**, 621; (*d*) J. Jurczak, S. Kaspryzk, P. Lipkowski, P. Salanski and T. Stankiewicz, *Tetrahedron*, 1993, **49**, 1488.
14 S. S. Basok, A. V. Bogatsky, N. G. Lukyanenko and L. K. Ostrovskaya, *Synth. Commun.*, 1984, **2**, 138.
15 A. V. Bogatskii, T. I. Kirichenko and N. G. Lukyanenko, *J. Org. Chem. USSR*, 1981, **17**, 944.
16 M. Buttafava, A. Manfredi and S. Quici, *J. Org. Chem.*, 1996, **61**, 3870.
17 (*a*) J. M. Lehn, S. H. Pine, E. Watanabe and A. K. Wilard, *J. Am. Chem. Soc.*, 1977, **99**, 6766; (*b*) S. R. Duff, K. Gu, M. W. Hosseini, J. M. Lehn and M. P. Mertes, *J. Org. Chem.*, 1987, **52**, 1662; (*c*) T. Deffo, K. B. Mertes, L. Qian and Z. Sun, *Tetrahedron Lett.*, 1990, **31**, 6469; (*d*) H. Fujioka, E. Kimura, T. Kioke, M. Kodama and Y. Kuramoto, *J. Org. Chem.*, 1990, **55**, 42; (*e*) J. S. Bradshaw, N. K. Dalley, R. M. Izatt, W. Jiang, K. E. Krakowiak and G. Wu, *J. Org. Chem.*, 1991, **56**, 2675; (*f*) C. Erk, *Liebigs Ann. Chem.*, 1991, 1083; (*g*) G. Brand, M. W. Hosseini and R. Ruppert, *Helv. Chim. Acta*, 1992, **75**, 721; (*h*) J. Buter, J. J. H. Edema and R. M. Kellog, *Tetrahedron*, 1994, **50**, 2095.
18 R. Haul and G. Dümbgen, *Chem.-Ing.-Tech.*, 1960, **32**, 349.
19 S. He, J. E. Oddo and M. B. Tomson, *Appl. Geochem.*, 1994, **9**, 561.
20 P. Risthaus, D. Bosbach, U. Becker and A. Putnis, *Colloids Surf., A*, 2001, **191**, 201.
21 D. Bosbach, C. Hall and A. Putnis, *Chem. Geol.*, 1998, **151**, 143.
22 C. M. Pina, U. Becker, P. Risthaus, D. Bosbach and A. Putnis, *Nature*, 1998, **395**, 483.
23 J. A. D. Wattis and P. V. Coveney, *J. Chem. Phys.*, 1997, **106**, 9122.